JOURNAL OF THERMOPHYSICS AND HEAT TRANSFER
Vol. 20, No. 3, July–September 2006

Modern Integral Method Calculation of Turbulent Boundary Layers

James Sucec*
University of Maine, Orono, Maine 04469-5711

Heat transfer in turbulent boundary layers, with zero or adverse pressure gradients, is calculated using modern integral methods. Inner variables are used with the velocity profile taken to be Coles's combined law of the wall and wake. The temperature profile used is the thermal law of wall and wake with an equilibrium wake strength function. The modeling employed takes into approximate account the dependence of velocity wake strength and thermal wake strength on the momentum thickness Reynolds number and the enthalpy thickness Reynolds number, respectively. Also, an attempt is made to incorporate the dependence of turbulent Prandtl number on pressure gradient into the model. Calculations are started at the leading edge, or beginning, of the surface with very small boundary-layer thicknesses, rather than matching the measured values of Stanton number and skin-friction coefficient at the location of the first experimental data point. Predictions are compared to experimental data which include both constant flux and constant temperature surfaces, some of which may have unheated starting lengths. There is reasonably good agreement between them for all but the case of very severe adverse pressure gradient.

Nomenclature

B	=	constant in the velocity profile, Eq. (1)
C_f	=	skin-friction coefficient, $2\tau_w/\rho u_s^2$
C_p	=	constant pressure specific heat
C_t	=	Prandtl number function in temperature profile, Eq. (2)
K	=	von Kármán constant, 0.41
L	=	reference length
P	=	local pressure
Pr	=	molecular Prandtl number
Pr_t	=	turbulent Prandtl number
q_w	=	surface heat flux
Re_x	=	local Reynolds number, $u_s x/\nu$
St_x	=	local Stanton number, $h_x/\rho c_p u_s$
T, T_w, T_s	=	local, wall, and freestream temperature, respectively
T^+	=	$(T_w - T)\rho C_p u^*/q_w$
T_s^+	=	value of T^+ in freestream
u, u_s	=	local and freestream x velocity component
u^*	=	friction velocity, $\sqrt{(\tau_w/\rho)}$
u^+	=	inner velocity, u/u^*
u_s^+	=	freestream value of u^+
X	=	nondimensional x coordinate, x/L
X_u	=	x_u/L, nondimensional unheated starting length
x	=	space coordinate along surface
x_u	=	unheated starting length
x_0	=	x value at start of calculations
y	=	space coordinate normal to surface
y^+	=	inner coordinate, yu^*/ν
β	=	Clauser parameter, $\delta^*(\mathrm{d}P/\mathrm{d}x)/\tau_w$
Δ	=	enthalpy thickness
δ, δ_t	=	local thickness of velocity and thermal boundary layer, respectively
δ^*	=	displacement thickness
δ^+, δ_t^+	=	value of y^+ at $y = \delta$ and δ_t
θ	=	momentum thickness
ν	=	kinematic viscosity
π, π_t	=	wake strength for velocity and temperature profiles, Eqs. (1) and (2)
ρ	=	mass density
τ_w	=	surface shear stress

Received 2 March 2005; revision received 24 August 2005; accepted for publication 1 September 2005.

*Professor, Department of Mechanical Engineering, Room 202.

Introduction

ONE way to calculate heat transfer in turbulent boundary layers is to employ the combined thermal law of the wall and wake. The work of So[1] supplied the information needed to estimate values of the thermal wake strength parameter π_t. This information was then used by Sucec[2] to construct a relation giving π_t as a function of a pressure gradient parameter β and the turbulent Prandtl number Pr_t, and this was used in an integral method utilizing the thermal law of the wall and wake to predict the Stanton number distribution along a surface covered by a turbulent boundary layer.

Integral methods continue to play a role in engineering computations despite the use of numerical solutions using high-speed digital computers. A recent example of this is the closed-form solution of heat transfer in crossflow over a circular cylinder between parallel planes given by Khan et al.[3] The present work also uses an integral solution approach in which, unlike that of Sucec,[2] account is taken of the dependence of the velocity and thermal wake strength parameters, π and π_t, on the momentum thickness Reynolds number and the enthalpy thickness Reynolds number, respectively, by drawing on some earlier predictions by Fridman.[4] In addition, an approximate expression relating the turbulent Prandlt number in the log region to pressure gradient is proposed and used in the calculations. Finally, the heat transfer and fluid flow calculations are started at the leading edge of the surface or the positions at which heating starts, x_0, by use of very small thermal and hydrodynamic boundary-layer thicknesses. When these effects are utilized, the velocity and thermal laws of the wall and wake are used, in modern integral methods for turbulent flow, to solve the momentum and thermal energy equations in their integral forms to give predictions of the Stanton number distribution. These predictions are then compared to experimental data in both zero pressure gradient and some adverse pressure gradient turbulent boundary layers. The described refinements, which better represent the physics of the actual flow, result in significant increases in agreement of predictions with data, compared to those which do not account for these effects.

Analysis

The velocity and temperature profiles needed to solve the integral equations of motion and thermal energy are the combined laws of the wall and the wake, given next in inner coordinates u^+, y^+, and

T^+. Here u^+ is given by Coles law of wall and wake,

$$u^+ = (1/K)\,\ell_n\, y^+ + B + [2\pi(x)/K][3(y^+/\delta^+)^2 - 2(y^+/\delta^+)^3] \qquad 0 < y^+ \le \delta^+ \quad (1)$$

and for $y^+ > \delta^+$,

$$u^+ = u_s^+ = 1\Big/\sqrt{C_f/2}$$

The temperature profile T^+ where T^+ is $(T_w - T)\rho C_p u^*/q_w$, is given by the combined thermal law of wall and wake, namely,

$$T^+ = (Pr_t/K)\,\ell_n\, y^+ + C_t(Pr) + [2Pr_t\pi_t(x)/K] \times \left[3\left(y^+\Big/\delta_t^+\right)^2 - 2\left(y^+\Big/\delta_t^+\right)^3\right] \quad (2)$$

Relations for the Wake Strengths

The wake strength parameters, π and π_t, in Eqs. (1) and (2) are functions of the momentum thickness Reynolds number Re_θ and the enthalpy thickness Reynolds number Re_Δ, respectively. When these Reynolds numbers get large enough, π and π_t take on their "equilibrium" values, $\pi_{\rm eq}$ and $\pi_{t\rm eq}$. The velocity equilibrium wake values, $\pi_{\rm eq}$, used as a function of the Clauser parameter β were from Sucec and Oljaca,[5] namely,

$$\beta = -0.5 + 0.76\pi_{\rm eq} + 0.42\pi_{\rm eq}^2 \quad (3)$$

The thermal equilibrium wake strength, $\pi_{t\rm eq}$, which is a function of both β and turbulent Prandtl number Pr_t, is from Sucec[2] and is shown in Fig. 1. Cebeci and Bradshaw[6] give π in terms of momentum thickness Reynolds number, Re_θ, for zero pressure gradient as follows:

$$\pi = 0, \qquad 0 \le Re_\theta < 425$$
$$\pi = \pi_{\rm eq}\left[1 - \exp\left(-0.243\sqrt{Z_1} - 0.298Z_1\right)\right] \qquad 425 < {\rm Re}_\theta < 15,000$$
$$Z_1 = {\rm Re}_\theta/425 - 1 \quad (4)$$

Equation (4) approaches $\pi_{\rm eq}$ asymptotically at about $Re_\theta \approx 6000$, but Gad-el-Hak and Bandyopadhyay[7] point out that at $Re_\theta \approx 15{,}000$ π begins a slow decrease with increasing Reynolds number Re_θ.

Information and data relating π_t to $\pi_{t\rm eq}$ is rather limited. Faraco-Medeiros and Silva-Freire[8] present a curve of π_t plotted against enthalpy thickness Reynolds number Re_Δ based on their analysis of data by Blackwell.[9] They indicate that the limited number of experimental data points cause some degree of uncertainty in their values. Subramanian and Antonia[10] plotted π_t against momentum thickness Reynolds number Re_θ, instead of enthalpy thickness Reynolds number Re_Δ. In addition, they indicate that the value of $\pi_{t\rm eq} \approx 0.31$ for zero pressure gradient. (See Sucec[2] for a complete discussion of the controversial values of $\pi_{t\rm eq}$.) Fridman[4] in a numerical solution of the partial differential equations of mass, momentum, and energy, predicted $\pi_t = \pi_t(Re_\Delta)$ for zero pressure gradient and found that $\pi_{t\rm eq} \approx 0.627$, which is in good agreement with the value of 0.672 found by Sucec.[2] Hence, a curve fit was made to the results of Fridman[4] and is given as

$$\pi_t = \pi_{t\rm eq}[0.000477Re_\Delta], \qquad 0 < Re_\Delta < 348$$
$$\pi_t = \pi_{t\rm eq}[0.065 + 0.00029Re_\Delta], \qquad 348 < Re_\Delta < 1000$$
$$\pi_t = \pi_{t\rm eq}[1 - \exp(-0.00044109Re_\Delta)], \qquad Re_\Delta > 1000 \quad (5)$$

It was found that the ratio of $\pi_t/\pi_{t\rm eq}$ given by Eq. (5) was about 14% lower than the results of Faraco-Medeiros and Silva-Freire[8] and about 7% lower than those of Subramanian and Antonia[10] (after their results were converted from momentum thickness Reynolds number Re_θ values to enthalpy thickness Reynolds number Re_Δ values) for Re_Δ between 1000 and 5000.

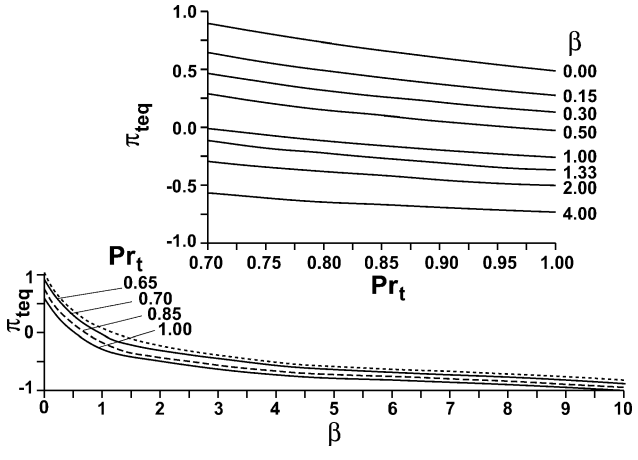

Fig. 1 Predicted thermal wake strength $\pi_{t\rm eq}$ variation with β and Prandtl number Pr_t.

Turbulent Prandtl number

As Kays[11] points out, there may be an effect of pressure gradient on the turbulent Prandtl number in the "log" region. Certainly, Figs. 6.5, 6.10, and 6.11 in Ref. 9 seem to indicate a decrease in turbulent Prandtl number Pr_t with increasing adverse pressure gradient for air. Some evidence for this also appears in Ref. 12. An attempt was made to quantify this effect, for pressure gradients characterized by $m = 0$, -0.15, and -0.20 in $U_s(x) \sim x^m$, from Blackwell's data. Turbulent Prandtl number Pr_t data given principally in Fig. 6.5 of Blackwell was averaged in the log region. This, along with the arguments in Ref. 2 for $Pr_t = 0.85$ for $m = 0$, led to $Pr_t = 0.85$, 0.7875, and 0.7625 for $m = 0$, -0.15, and -0.20, respectively. Then the following equation was fitted to these values.

$$Pr_t = 0.85 + 0.354166m - 0.41667m^2 \quad (6)$$

The direct numerical simulation (DNS) predictions of Wu and Durbin[13] for the distribution of turbulent Prandtl number Pr_t across the boundary layer are in good agreement with Blackwell's experimental results and lend further credence to them. In addition, some numerical experimentation in the present work indicated that the use of turbulent prandtl number Pr_t values from Eq. (6) led to the best predicted agreement of local Stanton numbers with experimental data.

Integral Method Solution for δ_t^+

The integral forms of the momentum equation in the x direction and of the thermal energy equation must be solved. The needed quantities, δ^+ and $C_f/2$, from the velocity field were found from a Runge–Kutta solution of the integral x momentum equation using Eq. (1) as the velocity profile. Details are given in Ref. 5. The integral equation for thermal energy was integrated along the x direction for specified wall flux $q_w(x)$,

$$\int_0^{\delta_t^+} u^+\left(T_s^+ - T^+\right)\mathrm{d}y^+ = \frac{u^*(x)}{\nu q_w(x)} \times \int_{x_0}^{x} q_w\,\mathrm{d}x + \frac{u^*(x)q_w(x_0)}{u^*(x_0)q_w(x)}\int_0^{\delta_{t0}^+} u^+\left(T_s^+ - T^+\right)\mathrm{d}y^+ \quad (7)$$

With u^+ and T^+ given by Eqs. (1) and (2), respectively, the integrations needed in Eq. (7) were carried out analytically and then the equation was solved for $\delta_t^+(x)$ by Newton's method. The calculation begins at x_0, where heating begins, by using a small value of $\delta_{tx_0}^+$ to simulate the essentially zero thermal-layer thickness there. Nonzero thicknesses are needed because of the natural log functions in Eqs. (1) and (2). The same procedure is used for the velocity field calculation, which begins either at x_0 or upstream of x_0 if there is an unheated starting length. For numerical purposes, if heating started at $x = 0$, $x = 0.000020$ m or ft was used because $x = 0.0$ causes Eq. (8) to become unbounded, and typically, values of $\delta^+ = \delta_t^+ = 30$ at this value of x. In some cases, these corresponded to values of

local Stanton number St_x and $C_f/2$ of 0.0092 and 0.00858. To verify that the solutions for the downstream skin friction and Stanton number were independent of these starting values, solutions were also found using $\delta^+ = \delta_t^+ = 1.010$ at $x = 0$, which led to a maximum difference in predicted local Stanton number St_x values of 0.25%.

For the experimental data cases where wall heat flux was specified, Eq. (7) is solved using the specified $q_w(x)$. However, many of the data cases were for constant wall temperature T_w. This was handled by simulating the constant T_w condition by using a flux distribution, $q_w(x)$, which gave approximately constant wall temperature. For constant freestream velocity over a constant T_w surface, information by Kays and Crawford[14] indicated the use of $q_w(x) \sim (x - x_0)^{-0.20}$. For the data sets, from the literature, where T_w was constant, but the freestream velocity varied with position x, that is, $U_s(x)$, a surface heat flux variation to give approximately constant wall temperature was developed from two sources, Ambrok[15] and Sucec.[16] For $U_s(x) \sim (ax + b)^m$, as it is for data cases in Refs. 9 and 12, flux expressions were derived, $q_w(x)$, from both of these sources, which gave approximately constant wall temperature. Using the expression given in Ref. 15, which is also given in Ref. 14, the following surface flux expression was developed:

$$q_w(x) \sim (ax + b)^m \left[(ax + b)^{1+m} - (ax_0 + b)^{1+m}\right]^{-0.20} \qquad (8)$$

Using Eq. (10) in Ref. 16, a simpler, but more approximate, flux expression to give T_w about constant when $U_s(x) \sim (ax + b)^m$ is

$$q_w(x) \sim (ax + b)^{-0.20 + 0.8m} \qquad (9)$$

From the standpoint of Stanton number predictions, there is little to choose between using Eq. (8) or the simpler surface flux expression (9) because the predicted Stanton numbers using Eqs. (8) and (9) differ by a maximum of 0.35%. However, use of the approximate flux expression (8) led to a more nearly constant wall temperature T_w along the surface, and so all results for isothermal cases where $U_s(x) = (a + bx)^m$, $m \neq 0$, are calculated using Eq. (8).

Stanton Number Calculation

Once the integral energy equation (7) has been solved for $\delta_t^+(x)$ by Newton's method, this is used in Eq. (2) to give T_s^+, and the definition of T_s^+ gives us the heat transfer law,

$$\sqrt{C_f/2}/St_x = (Pr_t/K)\,\ell_n\,\delta_t^+ + C_t(Pr) + 2(Pr_t/K)\pi_t \qquad (10)$$

In the calculations, the following values and expressions, needed in Eqs. (1), (2), and (10), were used: $B = 5.0$, $K = 0.41$, and $C_t(Pr) = 13.2Pr - 5.34$ (Ref. 14).

As mentioned earlier, the needed quantities form the velocity field solution, such as $C_f/2$, come from the fourth-order Runge–Kutta solution of an ordinary differential equation.[5] Lattice refinement studies were done. In one typical case, the final values of x direction lattice spacing, $\Delta x = 0.0056097$ m, was such that the maximum change in predicted local Staton number St_x values was 0.25% when the lattice spacing was cut in half. Most of the local Staton number St_x predictions exhibited changes significantly smaller than this. For instance, $\Delta x = 0.000625$ m was used for all of the cases of Taylor et al.,[17] and using half of this value changed the predicted local Stanton number St_x by only 0.005%.

Discussion and Results

Predicted results for the local Stanton number St_x for zero pressure gradient flows (U_s = constant) are presented both for no dependence of π and π_t on Reynolds numbers and also for accounting for the dependence of π and π_t on Reynolds numbers Re_θ and Re_Δ, respectively. The constant values of π and π_t used when ignoring their Reynolds number dependence were $\pi = 0.51266$ and $\pi_t = 0.6718$. This value of π_t corresponds to the use of the turbulent Prandtl number of 0.85. The calculations accounting for the Reynolds number dependency of π and π_t, on the other hand, employed the dependencies given in Eqs. (4) and (5). These predictions are compared to various sets of experimental data subsequently.

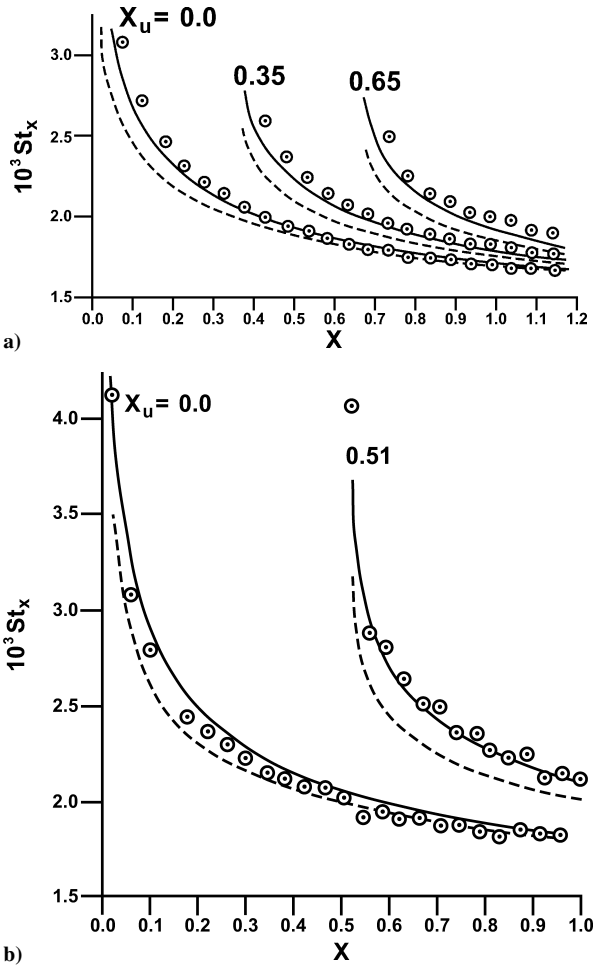

Fig. 2 Constant u_s: a) constant flux data, Taylor et al.[17] unheated lengths 0.0, 0.7, and 1.30 m left to right, (X_u = 0.0, 0.35, and 0.65) L = 2.0 m and b) isothermal surfaces, left curve's data, Moffat and Kays,[18] right curve's data, Orlando et al.,[12] unheated length 1.422 m, L = 2.77 m: ⊙, data and predictions; ——, π, π_t dependence on Reynolds numbers; and – – –, no dependence.

Figure 2 shows predictions using the Reynolds number dependence of both wake strengths as solid curves, the no-dependence results are given by the dashed curves, and the experimental data is shown as circled dots.

Figure 2a shows experimental data of Taylor et al.[17] for constant flux, zero pressure gradient surfaces. The lowest data set are for a completely heated surface ($0.21 \times 10^6 < Re_x < 9.87 \times 10^6$), the next highest data is for a surface with a 0.7-m unheated starting length ($1.31 \times 10^6 < Re_x < 4.11 \times 10^6$), whereas the uppermost data are for a surface with a 1.3-m unheated length ($2.37 \times 10^6 < Re_x < 4.13 \times 10^6$). The parameter X_u shown throughout is the nondimensional unheated starting length; thus, the values of 0.0, 0.35, and 0.65 in Fig. 2a. It is seen that the predictions that account for dependence of π and π_t on momentum thickness Reynolds number and enthalpy thickness Reynolds number, respectively (the solid curves), are in much better agreement with the data than are the predictions that use constant values of π and π_t. In the case of the 1.3-m starting length, the average difference between prediction and Stanton number data was reduced from 6.9 to 2.6%, whereas the maximum difference was reduced from 12.8 to 5.2% by the predictions that used the dependence of the wake strengths, π and π_t, on the Reynolds numbers.

In Fig. 2b, the upper data set is from Orlando et al.[12] for U_s = constant, a 1.27-m unheated length ($8.2 \times 10^5 < Re_x < 15.7 \times 10^5$) followed by a constant temperature surface. The improvement in predictions of local Stanton number St_x, when using the dependence of π and π_t on Reynolds numbers, is quite dramatic for this case. The lower data set is from Moffat and Kays,[18] for a fully heated

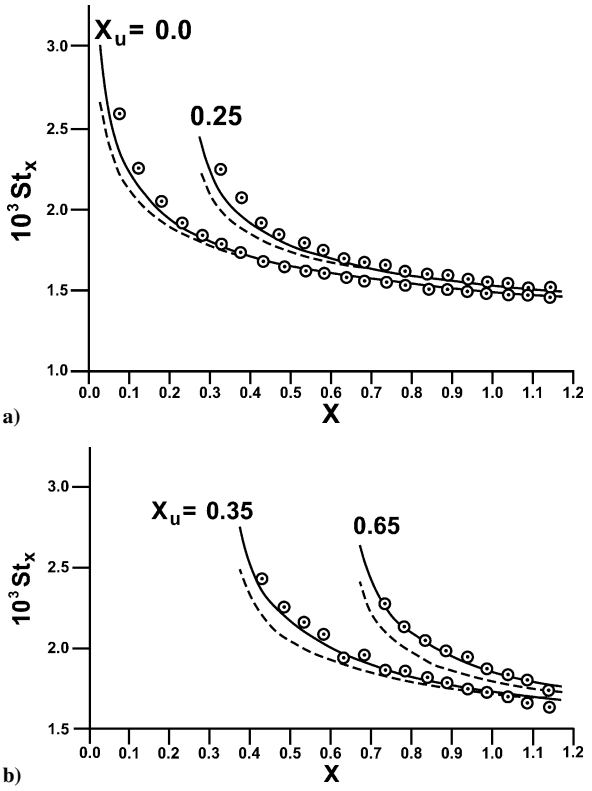

Fig. 3 Constant u_s: a) constant flux, unheated starting lengths 0.0 and 0.5 m, left to right and b) isothermal surface after unheated lengths 0.7 and 1.30 m, left to right; all data Taylor et al.,[17] $L = 2.0$ m: ⊙, data and predictions; ——, π, π_t dependence on Reynolds numbers; and – – –, no dependence.

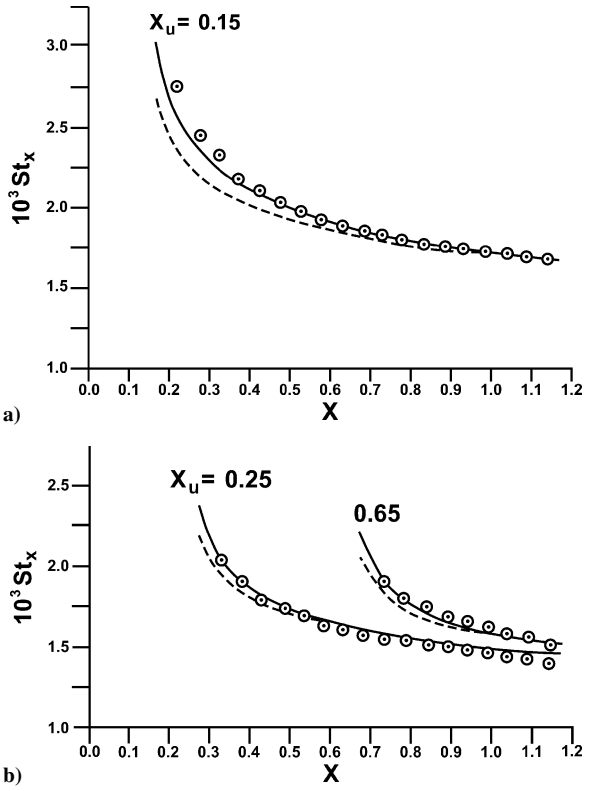

Fig. 4 Constant u_s: a) constant flux after unheated length 0.3 m and b) isothermal surface after unheated length 0.5 and 1.30 m left to right; all data Taylor et al.,[17] $L = 2.0$ m: ⊙, data and predictions; ——, π, π_t dependence on Reynolds numbers; and – – –, no dependence.

isothermal surface ($4.55 \times 10^4 < Re_x < 2.14 \times 10^6$). Here the predictions using variable wake strengths did not make that large a difference. The average of the predictions led to a 0.3% better agreement with data than the constant π and π_t predictions. However, the maximum difference was reduced from 15 to 5.6%. The reduction in maximum difference between predictions and data generally occurs for data at the lowest X values because this is where enthalpy thickness Reynolds number Re_Δ is smallest and gives the biggest change in π_t due to the low values of the enthalpy thickness Reynolds number here.

All of the data in Fig. 3 are from Taylor et al.[17] for zero pressure gradient. In Fig. 3b, the two data sets are for surfaces with a 0.7- and 1.30-m, respectively, starting length ($1.33 \times 10^6 < Re_x < 4 \times 10^6$ and $2.4 \times 10^6 < Re_x < 4.1 \times 10^6$). This is followed by a constant temperature surface, whereas the data in Fig. 3a are for a fully heated surface ($0.21 \times 10^6 < Re_x < 9.87 \times 10^6$) and a surface with a 0.50-m unheated length ($2.29 \times 10^6 < Re_x < 9.78 \times 10^6$) with heated portions having the constant flux condition. Again, the predictions employing variable wake strengths shown are in better agreement with data than those using constant values of π and π_t. The lowest data sets in Figs. 3a and 2a are both for fully heated constant flux surfaces from Taylor et al.[17] The difference in them is that the Reynolds numbers in Fig. 2a are only about 40% as large as those in Fig. 3a. The data on the Fig. 3a curve have x Reynolds numbers ranging from 0.21×10^6 to 9.87×10^6. This explains the coalescence of the dashed and solid curves in Fig. 3a at about $X = 0.30$, whereas it takes a value of about $X = 0.9$ for this to happen in Fig. 2a because the lower values of enthalpy thickness Reynolds number Re_Δ are reflected in a wake strength, π_t, which is farther away from the ultimate equilibrium value π_{teq}.

The data in Fig. 4 are also from Taylor et al.,[17] with the data set in Fig. 4a being for a constant flux surface with a 0.30-m unheated starting length ($0.61 \times 10^6 < Re_x < 4.1 \times 10^6$), whereas the data sets in Fig. 4b are for isothermal surfaces having a 0.50-m unheated length ($2.31 \times 10^6 < Re_x < 9.5 \times 10^6$) for the lowest data set and a 1.30-m unheated length ($5.95 \times 10^6 < Re_x < 9.87 \times 10^6$) for the higher data set. Again, the use of wake strengths that vary with Reynolds numbers gives closer agreement of predictions with data than does the use of constant values of π and π_t. Once again, the Reynolds number effect is seen in that the data set in Fig. 4a has Reynolds numbers less than one-half of their value for the lowest data set in Fig. 4b; thus, the predictions using constant π and π_t values coalesce with those using the Reynolds numbers dependencies in a much shorter distance, $X = 0.55$, for the lowest data set than for the uppermost data set where $X \approx 0.95$.

In Fig. 5, both data sets (Taylor et al.[17]) are for specified wall temperature surfaces. Figure 5a has a 0.80-m unheated length ($3.36 \times 10^6 < Re_x < 9.87 \times 10^6$) preceding the constant surface temperature, whereas Fig. 5b is for a fully heated surface ($0.087 \times 10^6 < Re_x < 4.11 \times 10^6$). Notable in Fig. 5b is neither the predictions using variable wake strengths nor those using constant wake strengths, except at values of $X < 0.20$, are in as good agreement with experimental data as all of the other cases from Taylor et al.[17] that were done. Yet, for other data sets involving a fully heated surface, that of Taylor et al.[17] for constant flux and that of Moffat and Kays[18] for constant wall temperature, both shown in Fig. 2, there was rather good agreement of present predictions and data.

The data in Fig. 6 are from Blackwell[9] for zero pressure gradient and a 0.152-m unheated length followed by a constant temperature surface ($0.28 \times 10^5 < Re_x < 12.6 \times 10^5$). Here, it is seen that the solution using Reynolds number dependence of π and π_t gives good agreement with data at the lowest values of X, the X values that corresponds to the lowest enthalpy thickness Reynolds numbers. However, at higher values of X, the constant π and π_t solution gives better agreement with data. Overall, the constant wake strength solution is, on the average, 2.5% closer to the data than is the variable wake strength solution, whereas the variable wake strength solution reduces the maximum discrepancy with data from 9 to 5.5%. Yet, even for this data set, there is some additional evidence in favor of the variable wake strengths solution, namely, that the surface heat flux variation used to simulate the constant temperature surface gave a much more uniform surface temperature than did the constant π and π_t

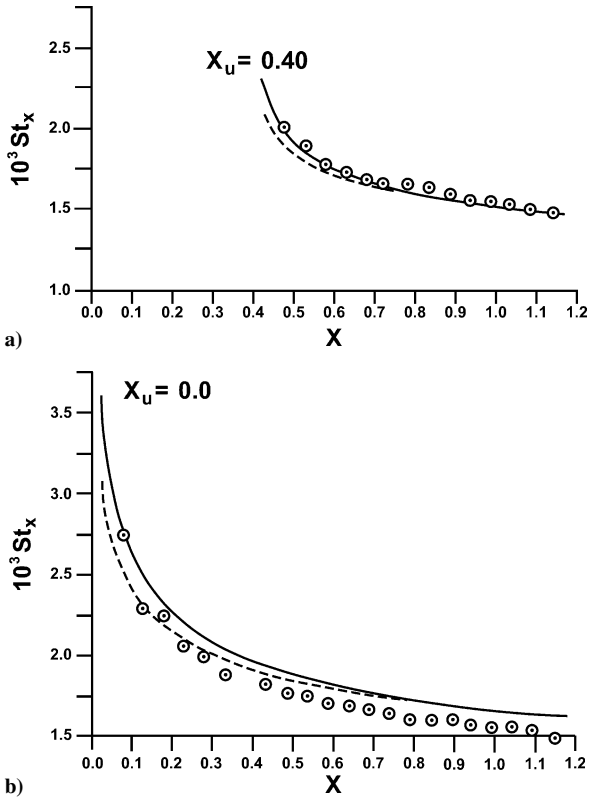

Fig. 5 Constant u_s, isothermal surface after unheated lengths 0.8 and 0.0 m, top to bottom; data Taylor et al.,[17] $L = 2.0$ m: ⊙, data and predictions; ——, π, π_t dependence on Reynolds numbers; and – – –, no dependence.

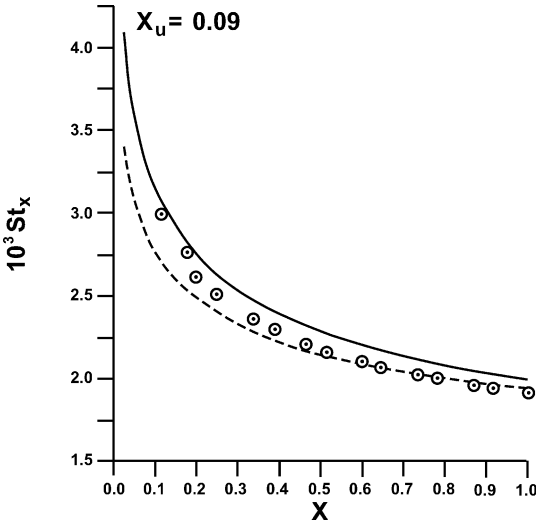

Fig. 6 Constant u_s, isothermal after unheated length of 0.152 m, Blackwell,[9] $L = 2.286$ m: ⊙, data and predictions; ——, π, π_t dependence on Reynolds numbers; and – – –, no dependence.

solution. In fact, the same thing was true for every data set in Figs. 2–6, all zero pressure gradient cases, thus lending more credibility to the variable wake strength, with Reynolds numbers, approach.

There is, however, one additional factor that affects thermal wake strength, in a zero pressure gradient boundary layer, that has not been accounted for. Fridman[4] predicts a reduction in the π_t when there is an unheated starting length. This is due to the growth of the thermal boundary layer within the thicker hydrodynamic boundary layer. The turbulence within the hydrodynamic layer, at the outer edge of the thermal layer, has somewhat the same effect as freestream turbulence has on a fully heated boundary layer, namely, to depress the value of the wake strength. There appears to be very little quantitative date available on this effect.

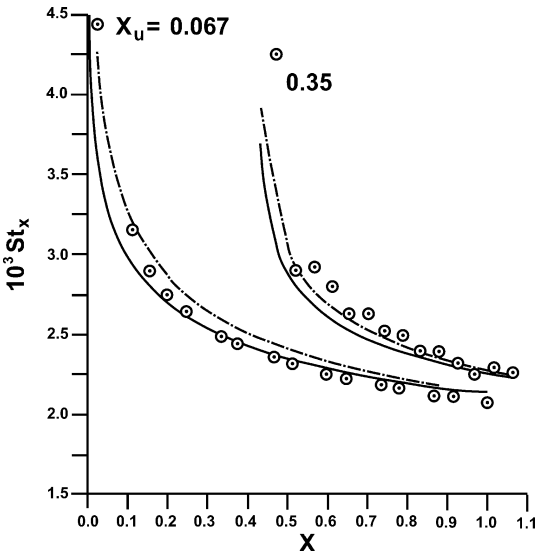

Fig. 7 Isothermal surface after unheated lengths 0.152 and 0.965 m, left to right, $u_s \sim x^{-0.15}$; left data, Blackwell,[9] $L = 2.28$ m and right data set, Orlando et al.,[12] $L = 2.77$ m: ⊙, data and predictions; · – · –, π, π_t dependence on Reynolds numbers; and ——, no dependence.

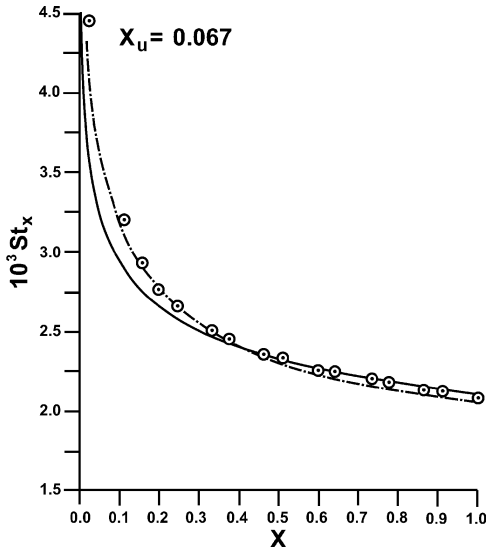

Fig. 8 Isothermal after 0.152-m unheated length; $u_s \sim x^{-0.20}$, Blackwell,[9] $L = 2.28$ m: ⊙, data and predictions; · – · –, π, π_t dependence on Reynolds numbers; and ——, no dependence.

Figures 7–9 have data and predictions for adverse pressure gradients. In Figs. 7–9, the solid curves are the predictions for no dependence of π and π_t on Reynolds numbers Re_θ and Re_Δ, whereas the dashed–dot curves are predictions using the dependence of π and π_t on Reynolds numbers. The dependence used, given by Eqs. (4) and (5), is the same one used for zero pressure gradient. This, of course, may not have complete validity for the adverse pressure gradient cases.

Figure 7 results are for a mild adverse pressure gradient, one characterized by $U_s(x) \sim x^{-0.15}$, thus, Eq. (6) suggests use of $Pr_t = 0.7875$. For the lower set of data points, the predictions without the Reynolds number dependence of π and π_t are in slightly better agreement with the bulk of the data points, although the predictions using the zero pressure gradient dependency are in much better agreement with the first two data points, the ones with the smallest values of Reynolds numbers Re_θ and Re_Δ. The lower set of data are from Blackwell[9] for a 0.152-m unheated length ($0.78 \times 10^5 < Re_x < 8.25 \times 10^5$) followed by an isothermal surface. On the other hand, the upper set of data from Orlando et al.,[12] with an unheated starting length of 0.965 m ($3.67 \times 10^5 < Re_x < 8.64 \times 10^5$) show better agreement with the predictions using the

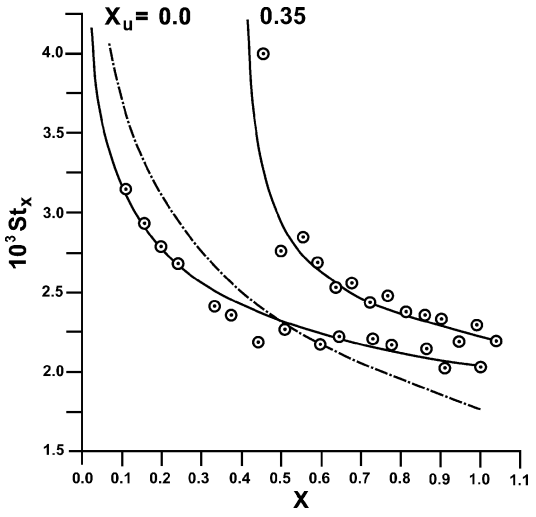

Fig. 9 Isothermal surface after unheated lengths 0.0 and 0.965 m, left to right, $u_s \sim x^{-0.275}$; data Orlando et al.,[12] $L = 2.77$ m: ⊙, data and predictions; – · – ·–, π, π_t dependence on Reynolds numbers, and ——, no dependence.

dependence of π and π_t on Reynolds numbers Re_θ and Re_Δ, the dashed–dot curve.

Figure 8 contains data from Blackwell[9] for a strong adverse pressure gradient where $U_s(x) \sim x^{-0.20}$ with 0.15-m unheated length followed by a constant temperature surface ($0.86 \times 10^5 < Re_x < 7.9 \times 10^5$). A value of $Pr_t = 0.7625$, found from Eq. (6) was used in the predictions. The predictions using the dependence of wake strengths on Reynolds numbers are in good agreement with the data. Clearly, the predictions using the Reynolds number dependencies (the dashed–dot curve) are closer to the data at low X, where Reynolds numbers Re_θ and Re_Δ are low for the same reasons explained earlier.

Shown in Fig. 9 are results for a very severe adverse pressure gradient. These data are from Orlando et al.[12] where $U_s(x) \sim x^{-0.275}$. This value of $m = -0.275$ in x^m gives a Pr_t very close to 0.70 from Eq. (6). The lowest data set and corresponding predictive curves are for a fully heated isothermal surface ($3.26 \times 10^5 < Re_x < 6.3 \times 10^5$). The behavior here is quite the opposite of that exhibited for the mild and the strong adverse pressure gradients in Figs. 7 and 8, where there was good agreement between the data and the predictions using the dependence of π and π_t on Reynolds numbers. In Fig. 9, the predictions using wake strengths independent of momentum and enthalpy thickness Reynolds numbers (solid curves) are better than the ones that employ the Reynolds number dependencies. The same is also true for the higher data set that has the same very severe adverse pressure gradient, but with a 0.965-m unheated length and where the predictions with Reynolds numbers dependence were not even plotted. This contrasts sharply with the good results achieved in Fig. 7 for the mild adverse pressure gradient data, the upper data set that is also from Orlando et al.,[12] and also for a 0.965-m unheated length.

Thus, although the zero pressure gradient dependence of wake strengths, π and π_t, on momentum and enthalpy thickness Reynolds numbers worked reasonably well for the mild and strong adverse pressure gradients, this did not extend to the very severe adverse pressure gradient of the data in Fig. 9.

The reasons as to why this is the case must perhaps wait either for more experimental data or for DNS results of heat transfer in very severe adverse pressure gradients. Specifically, what is needed is evidence relating the Reynolds number dependence of π and π_t to their equilibrium values π_{eq} (β) and $\pi_{t\text{eq}}$ (β, Pr_t) for turbulent boundary layers with severe adverse pressure gradients.

Conclusions

An expression relating the strength of the thermal wake, π_t, to its equilibrium value $\pi_{t\text{eq}}$ as a function of enthalpy thickness Reynolds number has been developed for zero pressure gradient flows. It is then used, along with the velocity wake strength π as a function of momentum thickness Reynolds number, in a integral method solution for the local Stanton number. The predicted Stanton numbers agreed reasonably well with experimental data and the results showed improved agreement with data when the Reynolds number dependencies of the two wake strengths were used, rather than simply ignoring this dependence and using the constant values of π and π_t appropriate for zero pressure gradient turbulent flows.

Also developed is an approximate equation relating turbulent Prandtl number Pr_t to the strength of adverse pressure gradients. This was used in the predictions of Stanton numbers for several adverse pressure gradients, ranging from mild to severe, and resulted in fairly good agreement with experimental data.

The zero pressure gradient relations between wake strengths and Reynolds numbers were also used in the predictions of the adverse pressure gradient cases.

References

[1]So, R. M. C., "Pressure Gradient Effects on Reynolds Analogy for Constant Property Equilibrium Turbulent Boundary Layers," *International Journal of Heat and Mass Transfer*, Vol. 37, No. 1, 1994, pp. 27–41.

[2]Sucec, J., "Calculation of Turbulent Boundary Layers Using Equilibrium Thermal Wakes," *Proceedings of the IMECE 2002 ASME International Mechanical Engineering Congress and Exposition* [CD-ROM], Vol. 1, Heat Transfer, American Society of Mechanical Engineers, New York, 2002, pp. 1–7.

[3]Khan, W. A., Culham, J. R., and Yovanovich, M. M., "Fluid Flow and Heat Transfer from a Cylinder Between Parallel Planes,"*Journal of Thermophysics and Heat Transfer*, Vol. 18, No. 3, 2004, pp. 395–403.

[4]Fridman, E., "Heat Transfer and Temperature Distribution in a Turbulent Flow over a Flat Plate with an Unheated Starting Length," HTD Vol. 346, *Proceedings of the 1997 National Heat Transfer Conference*, Vol. 8, American Society of Mechanical Engineers, New York, 1997, pp. 127–132.

[5]Sucec, J., and Oljaca, M., "Calculation of Turbulent Boundary Layers with Transpiration and Pressure Gradient Effects," *International Journal of Heat and Mass Transfer*, Vol. 38, No. 15, 1995, pp. 2855–2862.

[6]Cebeci, T., and Bradshaw, P., *Physical and Computational Aspects of Convective Heat Transfer*, Springer-Verlag, New York, 1984, p. 188.

[7]Gad-el-Hak, M., and Bandyopadhyay, P. R., "Reynolds Number Effects in Wall Bounded Turbulent Flows," *Applied Mechanics Reviews*, Vol. 47, No. 8, 1994, pp. 307–365.

[8]Faraco-Medeiros, M. A., and Silva-Freire, A. P., "The Transfer of Heat in Turbulent Boundary Layers with Injection or Suction: Universal Laws and Stanton Number Equations," *International Journal of Heat Mass Transfer*, Vol. 35, No. 4, 1992, pp. 991–995.

[9]Blackwell, B. F., "The Turbulent Boundary Layer on a Porous Plate: An Experimental Study of the Heat Transfer Behavior with Adverse Pressure Gradients," Ph.D. Dissertation, Dept. of Mechanical Engineering, Stanford Univ., Stanford, CA, Aug. 1972.

[10]Subramanian, C. S., and Antonia, R. A., "Effect of Reynolds Number on a Slightly Heated Turbulent Boundary Layer," *International Journal of Heat and Mass Transfer*, Vol. 24, No. 11, 1981, pp. 1833–1846.

[11]Kays, W. M., "Turbulent Prandtl Number—Where Are We?" *Journal of Heat Transfer*, Vol. 116, No. 2, 1994, pp. 284–295.

[12]Orlando, A. F., Moffat, R. J., and Kays, W. M., "Turbulent Transport of Heat and Momentum in a Boundary Layer Subject to Deceleration, Suction and Variable Wall Temperature," Thermosciences Div. Rept. HMT-17, Stanford Univ., Stanford, CA, May 1974.

[13]Wu, X., and Durbin, P. A., "Numerical Simulation of Heat Transfer in a Transitional Boundary Layer with Passing Wakes," *Journal of Heat Transfer*, Vol. 122, No. 2, 2000, pp. 248–257.

[14]Kays, W. M., and Crawford, M. E., *Convective Heat and Mass Transfer*, 3rd ed., McGraw–Hill, New York, 1993, Chap. 13.

[15]Ambrok, G. S., "Approximate Solutions of the Equations for the Thermal Boundary Layer with Variations in Boundary Layer Structure," *Soviet Physics—Technical Physics*, Vol. 2, No. 9, 1954, pp. 1979–1986.

[16]Sucec, J., "Approximate Analytical Solution to Forced Convection with Arbitrary Surface Heat Flux," *International Journal of Heat and Mass Transfer*, Vol. 32, No. 6, 1989, pp. 1189–1192.

[17]Taylor, R. P., Love, P. H., Coleman, H. W., and Hosni, M. H., "The Effect of Step Changes in the Thermal Boundary Condition on Heat Transfer in the Incompressible Flat Plate Turbulent Boundary Layer," HTD Vol. 107, *Proceedings of the 1989 National Heat Transfer Conference*, American Society of Mechanical Engineers, New York, 1989, pp. 9–16.

[18]Moffat, R. J., and Kays, W. M., "The Turbulent Boundary Layer on a Porous Plate: Experimental Heat Transfer with Uniform Blowing and Suction," *International Journal of Heat and Mass Transfer*, Vol. 11, 1968, pp. 1547–1566.